Desalination and Water Treatment
www.deswater.com

doi: 10.1080/19443994.2016.1185042

57 (2016) 28323–28339
December

Taylor & Francis
Taylor & Francis Group

Removal of arsenic and selenium from aqueous solutions using magnetic iron oxide nanoparticle/multi-walled carbon nanotube adsorbents

Chang-Gu Lee[a], Song-Bae Kim[b,c,d,*]

[a]*Center for Water Resource Cycle Research, Korea Institute of Science and Technology, Seoul 02792, Republic of Korea, Tel. +82 2 958 5822; email: changgu@kist.re.kr*
[b]*Environmental Functional Materials and Water Treatment Laboratory, Seoul National University, Seoul 08826, Republic of Korea, Tel. +82 2 880 4587; email: songbkim@snu.ac.kr*
[c]*Department of Rural Systems Engineering and Research Institute for Agriculture and Life Sciences, Seoul National University, Seoul 08826, Republic of Korea*
[d]*Institute of Green Bio Science and Technology, Seoul National University, Pyeongchang 25354, Republic of Korea*

Received 3 February 2016; Accepted 25 April 2016

ABSTRACT

The removal of arsenic (As(III), As(V)) and selenium (Se(IV), Se(VI)) from aqueous solutions was examined in batch systems using magnetic iron oxide nanoparticles/multi-walled carbon nanotubes (MIO–MWCNTs) as adsorbents. The effects of reaction time, temperature, solution pH, initial contaminant concentration, and interfering anions were investigated. Kinetic model analyses demonstrate that the Elovich model was the most suitable for describing the As(III) and As(V) data, whereas the pseudo-second-order model provided the best fit for the Se(IV) and Se(VI) data. Thermodynamic analyses indicate that As(III) adsorption was endothermic, while As(V) adsorption was exothermic (As(III): $\Delta H^\circ = 56.930$ kJ/mol; As(V): $\Delta H^\circ = -78.501$ kJ/mol). Meanwhile, the adsorption of Se(IV) and Se(VI) was exothermic (Se(IV): $\Delta H^\circ = -6.921$ kJ/mol; Se(VI): $\Delta H^\circ = -1.599$ kJ/mol). The adsorption capacity of As(III) increased gradually from 4.25 to 6.95 mg/g between pH 1.6 and 6.8, while the adsorption capacity of As(V) decreased from 9.09 to 3.69 mg/g as pH increased from 1.7 to 7.9. The adsorption capacity for Se(IV) decreased from 9.45 to 4.65 mg/g with a rise in pH from 1.8 to 7.1, and the adsorption capacity for Se(VI) decreased gradually from 6.09 to 0.11 mg/g between pH 1.9 and 7.0. Interfering anions such as phosphate and carbonate significantly reduced the removal of arsenic and selenium. Equilibrium model analyses indicate that the Freundlich model was the most appropriate for the As(III) and As(V) data, whereas the Redlich–Peterson model gave the best fit for the Se(IV) and Se(VI) data. The maximum adsorption capacity from the Langmuir model (mg/g) was in the order of As(V) (16.85) > As(III) (14.26) > Se(IV) (13.08) > Se(VI) (6.13).

Keywords: Adsorbents; Arsenic; Magnetic iron oxide nanoparticles; Multi-walled carbon nanotubes; Selenium

*Corresponding author.

1. Introduction

The contamination of drinking water resources by organic and inorganic contaminants is a serious environmental problem around the globe. Among various inorganic pollutants in surface and ground waters, arsenic (As) and selenium (Se) are major ones, causing a threat to human health. Arsenic is one of abundant elements in the earth's crust, and it is naturally dissolved in water through weathering [1]. Anthropogenic activities, such as mining and pesticide application, are also sources of arsenic in water. Water contamination by arsenic has been reported around the world and is especially serious in certain parts of Asia, such as Bangladesh and India [1,2]. Long-term exposure to drinking water containing arsenic can cause increased occurrences of skin, lung, bladder, and kidney cancers [2]. Therefore, the World Health Organization recommends a maximum contaminant level of 10 μg/L for drinking water. However, the toxicity and transport properties of arsenic strongly depend on their chemical form. The forms of arsenic occur with valance states of −3, 0, 3, and 5. Most arsenic exists as arsenite (AsO_3^{3-}, As(III)) and arsenate (AsO_4^{3-}, As(V)) in water [3], and As(III) is more toxic than As(V). Meanwhile, selenium is a natural trace element, known to be an essential nutrient for animals and humans. Selenium contamination in drinking water is currently of concern because of the narrow range between selenium deficiency and toxicity to humans [4,5]. Selenium is introduced into water from various sources including agricultural activities, fossil fuel combustion, and other industrial effluents [6]. Selenium exists in valance state of −2, 0, 4, and 6 and has several organic forms [7]. Because higher valance forms of selenium are more water soluble, selenite (SeO_3^{2-}, Se(IV)) and selenate (SeO_4^{2-}, Se(VI)) are the predominant forms found in water, and Se(IV) is more toxic than Se(VI) [5,8]. The United States Environmental Protection Agency has established the maximum selenium contaminant level in drinking water to be 50 μg/L [4].

Various treatment techniques have been used for the removal of inorganic contaminants from water, including coagulation, chemical reduction, ion exchange, adsorption, and membrane filtration [4,5,9]. Adsorption has been widely used because of its cost-effectiveness and simplicity of operation [4,10–12]. Carbon nanotubes (CNTs) are carbon-based nanomaterials, which have been widely used as adsorbents for the decontamination of aqueous solutions because of their nanoscale dimension, high aspect ratio, and large surface area [13,14]. CNTs have also served as a good support for iron oxide nanoparticles to prepare nanocomposites for the removal of various contaminants from water and wastewater [9,15]. Few researchers have studied the removal of arsenic and selenium by iron oxide–CNT composite. Tawabini et al. [16] modified multi-walled CNTs (MWCNTs) with iron oxide nanoparticles to enhance the removal of As(III) from water. Velickovic et al. [10] coated ethylenediamine-functionalized MWCNTs with goethite to remove As(III) and As(V) from drinking water. Wang et al. [17] deposited iron–nickel nanoparticles onto MWCNTs and used them for the removal of Se(IV) from water. Recently, researchers have immobilized magnetic iron oxide nanoparticles (MIO) such as maghemite (γ-Fe_2O_3) and magnetite (Fe_3O_4) on the surface of MWCNTs to synthesize magnetic composite adsorbents (MIO–MWCNTs) [18–20]. The MIO–MWCNTs could be used as adsorbents to remove contaminants from water and then separated from aqueous phase via magnetic separation. To our knowledge, limited studies have been reported in the literature for the removal of arsenic and selenium using the MIO–MWCNTs, including the removal of As(V) and As(III) [21] and As(V) [22] by the MIO–MWCNTs. Therefore, more research works are needed to improve understanding of the adsorption of arsenic and selenium to the MIO–MWCNTs.

The aim of this study was to investigate the removal of arsenic (As(III), As(V)) and selenium (Se (IV), Se(VI)) from aqueous solutions by the MIO–MWCNTs. Adsorption experiments were conducted in batch systems to examine the effect of reaction time, temperature, solution pH, initial contaminant concentration, and interfering anions on the removal of arsenic and selenium by the MIO–MWCNTs. Sorption kinetics, thermodynamics, and equilibrium isotherm models were used to analyze the experimental data.

2. Materials and methods

2.1. Preparation and characterization of MIO–MWCNTs

MWCNTs (CM-250; purity: 95%) were obtained from Hanwha Nanotech, Korea. Following previously published methods [23], the MWCNTs were placed in 70% nitric acid for 12 h at 70°C to increase their binding affinity to iron oxide nanoparticles by adding oxygen-containing functional groups (e.g. carboxylic group) to the MWCNT surfaces. The oxidized MWCNTs (O-MWCNTs) were filtered, washed with distilled water, and dried at 110°C for 6 h. The MIO–MWCNTs were prepared using the following procedures: a 400 mL solution (Fe(III)/Fe(II) molar ratio = 2) of $FeCl_3{\cdot}6H_2O$ (0.1 mol) and $FeSO_4{\cdot}7H_2O$ (0.05 mol) was prepared. Two grams of the O-MWCNTs were added to the

mixed solution and dispersed by ultrasonication for 4 h. A 6 M NaOH solution was later added dropwise until the solution pH reached 8. The solution was continually stirred for an additional 12 h to ensure reaction completion. The MIO–MWCNTs were subsequently washed with distilled water and dried at 150˚C for 6 h.

The surface morphology of the MIO–MWCNTs was characterized by various techniques. A transmission electron microscopy (TEM) analysis was conducted using a high-resolution transmission electron microscope (JEM-3010, JEOL, Tokyo, Japan). A field emission scanning electron microscopy (FESEM) analysis was performed using a field emission scanning electron microscope (Supra 55VP; Carl Zeiss, Oberkochen, Germany). A color mapping was performed with energy-dispersive X-ray spectrometry (Supra 55VP, Carl Zeiss, Oberkochen, Germany). The oxidation states of metal on the surface of the sample were analyzed using X-ray photoelectron spectroscopy (XPS Sigma Probe, Thermo VG, East Grinstead, UK) scans with monochromatic Al Kα radiation. In addition, a magnetic property was measured using a vibrating sample magnetometer (VSM 5–15, Toei Industry Co., Tokyo, Japan) with a field measurement range ±5.0 kOe at room temperature.

2.2. Batch experiments

Arsenic sorption experiments were conducted under batch conditions. The desired concentrations of As(III) and As(V) were prepared by diluting the stock solution (1,000 mg/L), which were made with sodium arsenite ($NaAsO_2$, 0.05 M, Fluka Sigma-Aldrich, St. Louis, MO, USA) and sodium arsenate ($Na_2HAsO_4{\cdot}7H_2O$, 98–102%, Sigma-Aldrich, St. Louis, MO, USA). All experiments were performed in triplicate under ambient conditions. The first set of experiments was conducted to examine the effect of reaction time on the removal of As(III) and As(V) by the O-MWCNTs and MIO–MWCNTs (initial arsenic concentration = 10 mg/L; temperature = 30˚C). The experiments were performed in 50 mL polypropylene conical tubes containing 1.0 g/L of the O-MWCNTs or MIO–MWCNTs and 30 mL of diluted arsenic solution. The tubes were shaken at 30˚C and 100 rpm using a shaking incubator (Daihan Science, Seoul, Korea). After the desired reaction time (15, 30, 45, 60, 120, 180, and 240 min), the adsorbents were separated from the solution by filtration through a 0.45 μm cellulose filter. The residual arsenic concentration was measured by inductively coupled plasma-atomic emission spectroscopy (ICP-AES) (Optima-4300, Perkin–Elmer, Waltham, Massachusetts, USA).

The second experiments were performed at 15 and 45˚C to examine the effect of temperature on the removal of As(III) and As(V) by the MIO–MWCNTs (initial As concentration = 10 mg/L). The third experiments were conducted to observe the effect of solution pH on the removal of As(III) and As(V) by the MIO–MWCNTs (initial As concentration = 10 mg/L; solution pH 1.6–7.9). The solution pH was adjusted using 0.1 M NaOH or 0.1 M HCl, which was monitored with a pH probe (9107BN, Thermo Scientific, Waltham, MA, USA). The fourth experiments were performed to examine the removal of As(III) and As(V) by the MIO–MWCNTs at different arsenic concentrations (initial As concentration = 5–100 mg/L). The fifth experiments were conducted to examine the effect of interfering anions on the removal of As(III) and As(V) by the MIO–MWCNTs (initial As concentration = 10 mg/L; interfering anions = 0.05 M $NaNO_3$, $NaHCO_3$, Na_2SO_4, NaH_2PO_4). Note that anions such as nitrate, bicarbonate, sulfate, and phosphate commonly exist in natural water.

Selenium sorption experiments were also performed following the same procedures as the arsenic sorption experiments. The desired concentrations of Se (IV) and Se(VI) were prepared by diluting stock solutions (1,000 mg/L), which were made with sodium selenite (Na_2SeO_3, 99%, Sigma-Aldrich, St. Louis, MO, USA) and sodium selenate (Na_2SeO_4, ≥95%, Sigma-Aldrich, St. Louis, MO, USA). In the first experiments, the removal of Se(IV) and Se(VI) by the O-MWCNTs and MIO–MWCNTs were performed at different reaction times (initial Se concentration = 10 mg/L; temperature = 30˚C). In the second, third, fourth, and fifth experiments, the removal of Se(IV) and Se(VI) by the MIO–MWCNTs were conducted at different temperatures (initial Se concentration = 10 mg/L; temperature = 15, 45˚C), solution pHs (initial Se concentration = 10 mg/L; pH 1.8–7.1), selenium concentrations (initial Se concentration = 5–100 mg/L), and interfering anions (initial Se concentration = 10 mg/L; interfering anions = 0.05 M $NaNO_3$, $NaHCO_3$, Na_2SO_4, NaH_2PO_4). The selenium concentration was also measured by ICP-AES.

2.3. Data analysis

Model parameters were estimated using MS Excel 2010 with the Solver add-in function. The determination coefficient (R^2) and chi-square coefficient (χ^2) were used to analyze the data and confirm the fit to the model. The equations of R^2 and χ^2 are:

$$R^2 = \frac{\sum_{i=1}^{m} (y_c - \overline{y_e})_i^2}{\sum_{i=1}^{m} (y_c - \overline{y_e})_i^2 + \sum_{i=1}^{m} (y_c - y_e)_i^2} \quad (1)$$

$$\chi^2 = \sum_{i=1}^{m} \left[\frac{(y_e - y_c)^2}{y_c} \right]_i \quad (2)$$

where y_c is the adsorption capacity calculated from the model, y_e is the adsorption capacity measured from the experiment, and $\overline{y}_e$ is the average measured adsorption capacity.

3. Results and discussion

3.1. Characteristics of MIO–MWCNTs

The digital image (Fig. 1) shows that the MIO–MWCNTs could be separated from the aqueous medium with an external permanent magnet. The saturation magnetization of the MIO–MWCNTs was determined to be 39.37 emu/g with a coercivity of 15.66 Oe. A more detailed microstructure of the MIO–MWCNTs was revealed by the TEM image (Fig. 2). The MWCNTs had a hollow inner tube diameter of 7–8 nm, outer diameter of 10–15 nm, and length of several hundred nanometers (Fig. 2(a)). The TEM image also demonstrates nanosized iron oxide particles with diameters ranging from 6 to 17 nm on the surface of the MWCNTs (Fig. 2(b)). They are slightly smaller than the iron oxide nanoparticles prepared without the MWCNTs [24]. The presence of the MWCNTs reduces the interactions between the iron oxide nanoparticles and subsequently their aggregation. Similar results were observed in the pure Fe_3O_4 nanoparticles and MWCNTs/Fe_3O_4 nanocomposites

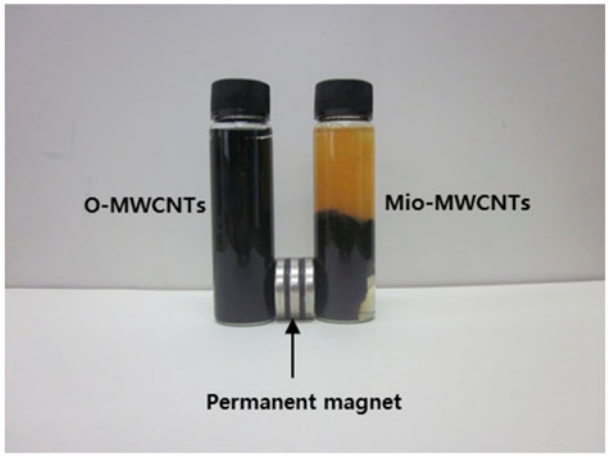

Fig. 1. Digital image of O-MWCNTs and MIO–MWCNTs under a permanent magnet.

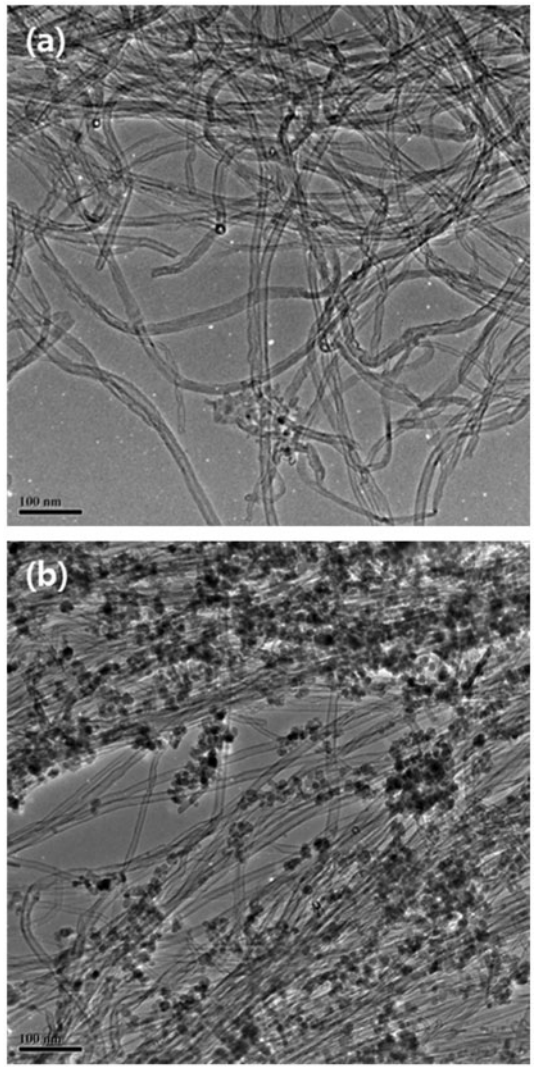

Fig. 2. TEM image (bar = 100 nm) of (a) O-MWCNTs and (b) MIO–MWCNTs.

[18]. Our previous research reported that the MIO–MWCNTs had a BET surface area of 119.09 m^2/g and a point of zero charge (pH_{PZC}) of 5.1 [25]. The surface morphology was also characterized by FESEM (Fig. 3). In the FESEM image of the MIO–MWCNTs (Fig. 3(a)), the MWCNTs are depicted as entangled with the iron oxide nanoparticles. Color mapping was performed to visualize the spatial distribution of carbon, oxygen, and iron (Fig. 3(b)–(d)). The mapping images show that all components were well-dispersed and consisted of 73.10 wt% carbon, 14.13 wt% oxygen, and 12.77 wt% iron on the surface of the sample.

The XPS spectra of the MIO–MWCNTs before and after sorption experiments are shown in Fig. 4. The photoelectron peaks at binding energies of 712, 531, and 285 eV in the wide scan (Fig. 4(a)) were attributed

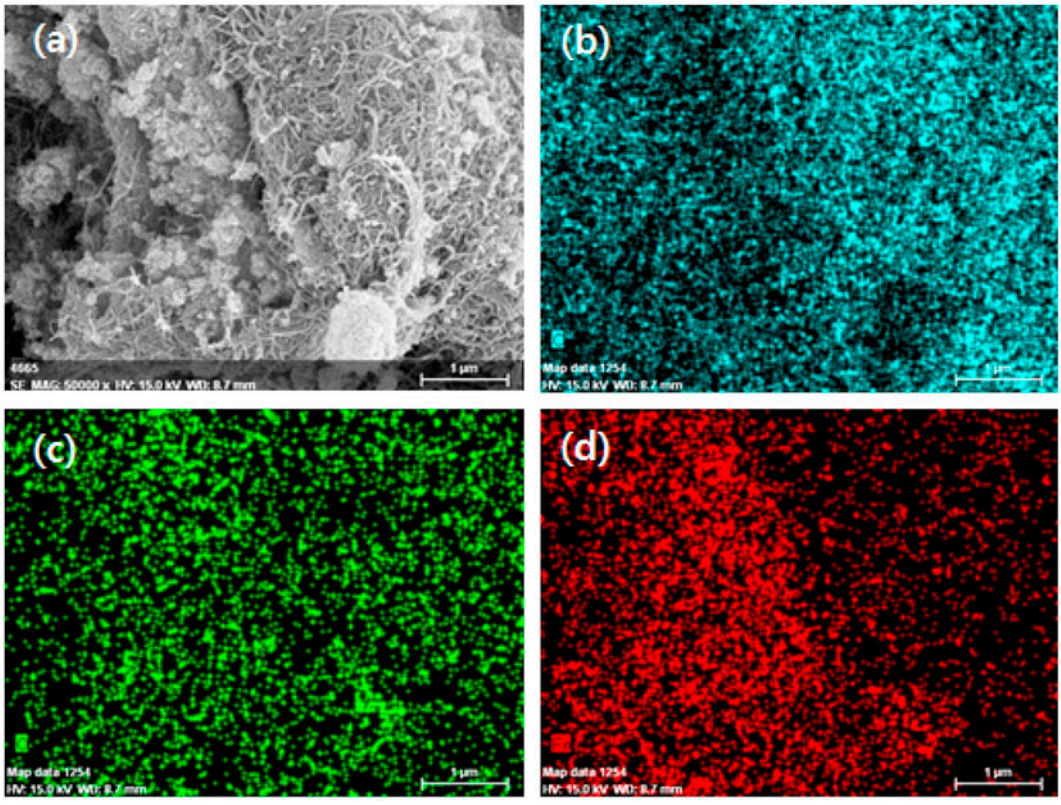

Fig. 3. Characteristics of MIO–MWCNTs: (a) FESEM image (bar = 1 μm), (b) color map of carbon (C), (c) color map of oxygen (O), and (d) color map of iron (Fe).

to Fe2p, O1s, and C1s, respectively, indicating that the nanocomposites were composed of iron, oxygen, and carbon. The high-resolution scan of the Fe2p region (Fig. 4(b)) marked two peaks at 724.6 and 711.2 eV, which agreed with the literature data for maghemite [26,27]. The spectrum of iron can cause interference in the arsenic and selenium spectrum during the XPS analysis. Therefore, several researchers have chosen the As3d and Se3d peaks to deconvolute the spectrum [28,29]. The high-resolution spectra of As3d and Se3d on the MIO–MWCNTs after reaction with arsenic and selenium are presented in Fig. 4(c) and (d), respectively. The binding energies of As(III) and As(V) were centered at 46.379 and 45.861 eV, while Se(IV) and Se (VI) were centered at 56.313 and 56.372 eV. No obvious change was observed for the Fe2p spectra before and after reaction with arsenic and selenium.

3.2. Effects of reaction time and temperature

The removal of As(III) and As(V) by the O-MWCNTs and MIO–MWCNTs is compared as a function of reaction time in Fig. 5(a) and (b), respectively. In the case of the MIO–MWCNTs, the adsorption capacities for As(III) and As(V) increased gradually with increasing reaction time until equilibrium was reached within 240 min. The adsorption capacity of As(III) augmented to 4.84 mg/g at 30 min of reaction time and further increased to 7.10 mg/g at 240 min (Fig. 5(a)). Meanwhile, the As(V) adsorption capacity was 5.96 mg/g at 30 min and increased to 9.56 mg/g at 240 min (Fig. 5(b)). For the O-MWCNTs, however, the adsorption capacities for As(III) and As (V) were negligible (under 0.22 mg/g at all times). After anchoring with the iron oxide nanoparticles, the adsorption capacity increased significantly, which indicates that the iron oxides played a major role in the sorption of arsenic. Our results also demonstrates that the adsorption capacity of As(V) by the MIO–MWCNTs (9.56 mg/g at 240 min) was greater than that of As(III) (7.10 mg/g at 240 min). These results are in agreement with the report of Ma et al. [3], who examined the adsorption of arsenic to CNTs and magnetic iron oxide/CNT composites, demonstrating that the adsorption capacity of As(V) was higher than that of As(III).

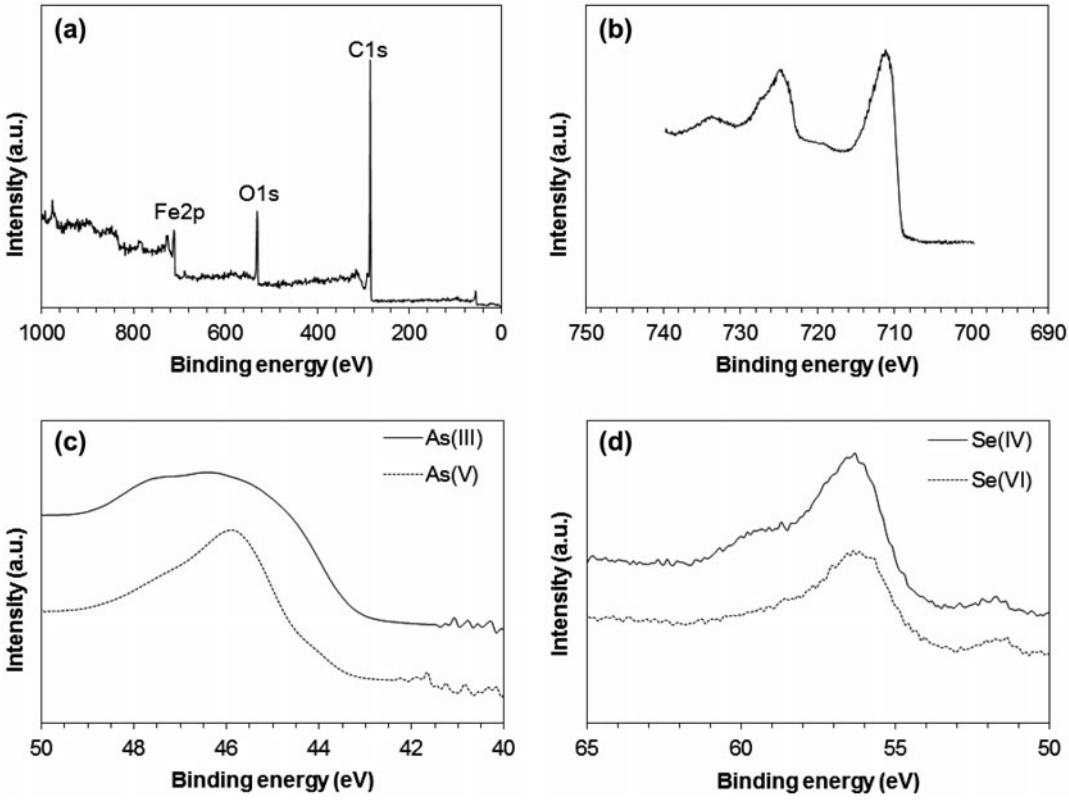

Fig. 4. XPS spectra of MIO–MWCNTs: (a) wide scan, (b) high-resolution scan of the Fe2p region, (c) high-resolution scan of the As3d region after sorption experiments, and (d) high-resolution scan of the Se3d region after sorption experiments.

The removal of Se(IV) and Se(VI) by the O-MWCNTs and MIO–MWCNTs are also compared in Fig. 5(c) and (d), respectively. The adsorption of Se (IV) and Se(VI) to the MIO–MWCNTs reached equilibrium within 240 min. In the case of Se(IV) (Fig. 5(c)), the adsorption capacity of the MIO–MWCNTs reached 6.81 mg/g after 30 min and increased gradually to 8.22 mg/g at 240 min. The Se(IV) adsorption capacity of the MIO–MWCNTs was 5.3–5.6 times greater than that of the O-MWCNTs, depending on the reaction time. A similar trend was observed for Se(VI) removal (Fig. 5(d)). The adsorption capacity of the MIO–MWCNTs was 3.68 mg/g after 30 min, reaching to 3.82 mg/g at 240 min. The Se(VI) adsorption capacity of the MIO–MWCNTs was 2.6–4.0 times greater than that of the O-MWCNTs, depending on the reaction time. Our results show that the iron oxide nanoparticles in the MIO–MWCNTs not only provide magnetic separation of the adsorbents, but also improve the adsorption capacity toward selenium.

In the case of the O-MWCNTs, the sorption capacity of Se(IV) (1.52 mg/g at 240 min) was slightly greater than that of Se(VI) (1.15 mg/g at 240 min). In contrast, the adsorption capacity of Se(IV) by the MIO–MWCNTs (8.22 mg/g at 240 min) was greater than that of Se(VI) (3.82 mg/g at 240 min), which indicates that the addition of iron oxide nanoparticles to MWCNTs improved the adsorption capacity of Se(IV) more than that of Se(VI). This result could be ascribed to the fact that Se(IV) has a higher binding affinity to iron oxide particles than Se(VI). Gonzalez et al. [4] performed a sorption study of Se(IV) and Se(VI) onto magnetite nanomaterial and reported that Se(IV) had a higher binding affinity to iron oxide than Se(VI) at pH 5 and 6. Martínez et al. [30] also examined the sorption of Se(IV) and Se(VI) to magnetite using batch experiments, demonstrating that Se(IV) had a higher sorption percentage than Se(VI) throughout the pH range between 2 and 12.

The effect of temperature on the removal of As(III) and As(V) by the MIO–MWCNTs is presented in Fig. 6(a) and (b), respectively. In the case of As(III), the adsorption capacity at 240 min increased from 7.24 to 9.87 mg/g with an increase in the temperature from 15 to 45°C (Fig. 6(a)). This result indicates that the adsorption of As(III) to the MIO–MWCNTs was an endothermic process. However, in the case of As(V), the adsorption capacity at 240 min decreased from

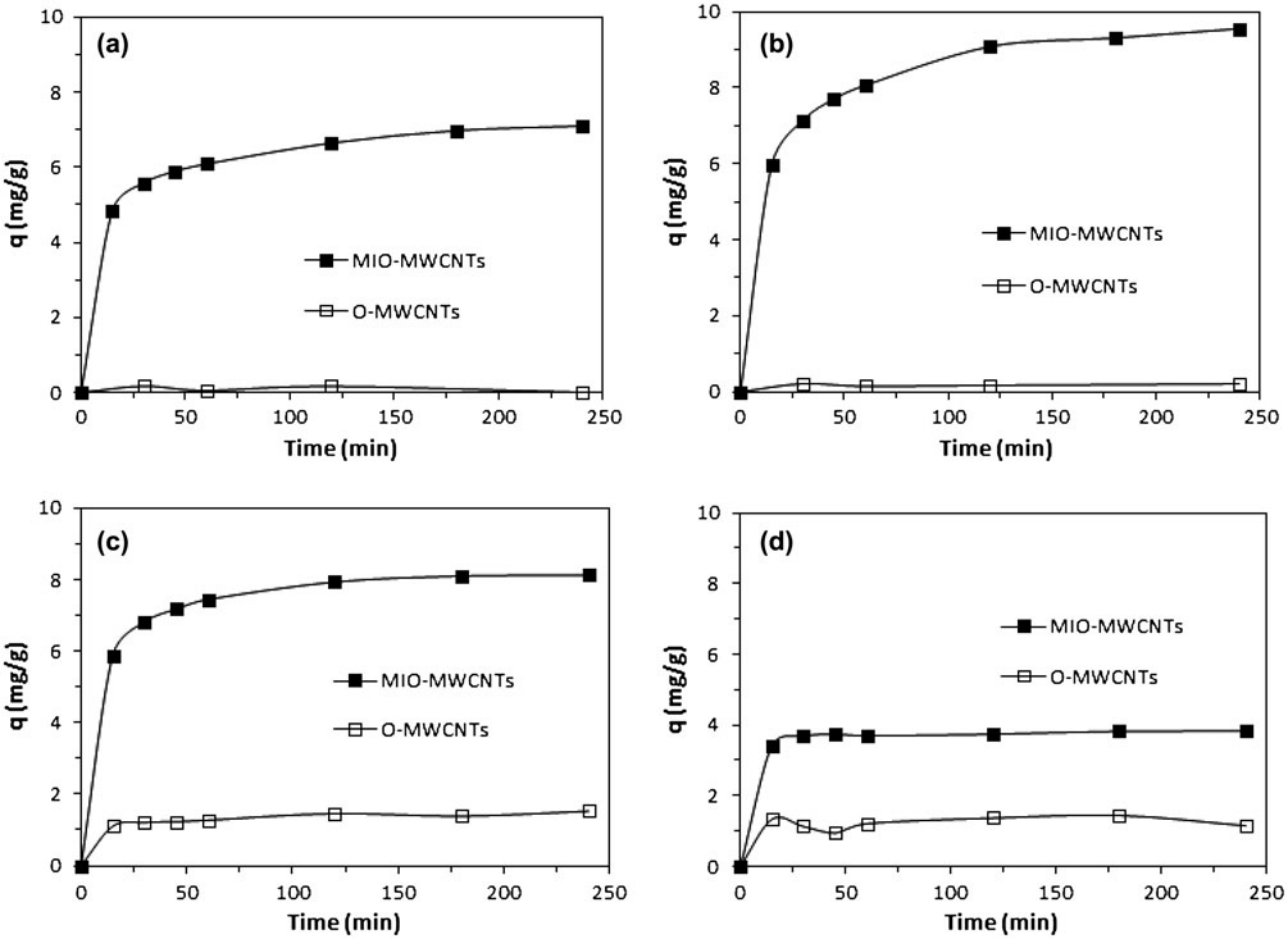

Fig. 5. Arsenic and selenium removal by O-MWCNTs and MIO–MWCNTs at different reaction times: (a) As(III), (b) As (V), (c) Se(IV), and (d) Se(VI).

8.37 to 7.19 mg/g with a rise in temperature from 15 to 45˚C (Fig. 6(b)). This result demonstrates that the adsorption of As(V) to the MIO–MWCNTs was an exothermic process. These different thermal properties were also observed for arsenic adsorption to Fe(III)–Si binary oxide adsorbent [31], where the adsorption of As(III) was endothermic, while the adsorption of As(V) was exothermic. The thermal properties of activated red mud were exothermic for As(III) and endothermic for As(V) [32]. These are interpreted as surface precipitation for the endothermic reaction and ligand exchange for the exothermic reaction [33,34].

The influence of temperature on the removal of Se(IV) and Se(VI) by the MIO–MWCNTs are shown in Fig. 6(c) and (d), respectively. The adsorption capacities for Se(IV) and Se(VI) decreased with increasing temperature. In the case of Se(IV), the adsorption capacity at 240 min decreased slightly from 8.38 to 8.12 mg/g with an increase in the temperature from 15 to 45˚C (Fig. 6(c)). In the case of Se(VI), the adsorption capacity at 240 min also decreased slightly from 3.95 to 3.79 mg/g with a rise in temperature from 15 to 45˚C (Fig. 6(d)). These results demonstrate that the adsorption of Se(IV) and Se(VI) to the MIO–MWCNTs was an exothermic process. Similar findings were reported in the literature. The adsorption capacity of Se(IV) on iron oxide [35] and magnetite [36] decreased with increasing temperature. At higher temperature, the lower the amount of Se(VI) adsorbed on the goethite surface [37].

3.3. Kinetic and thermodynamic model analyses

The experimental data in Fig. 6 were analyzed using the following pseudo-first-order (Eq. (3)), pseudo-second-order (Eq. (4)), and Elovich (Eq. (5)) kinetic models:

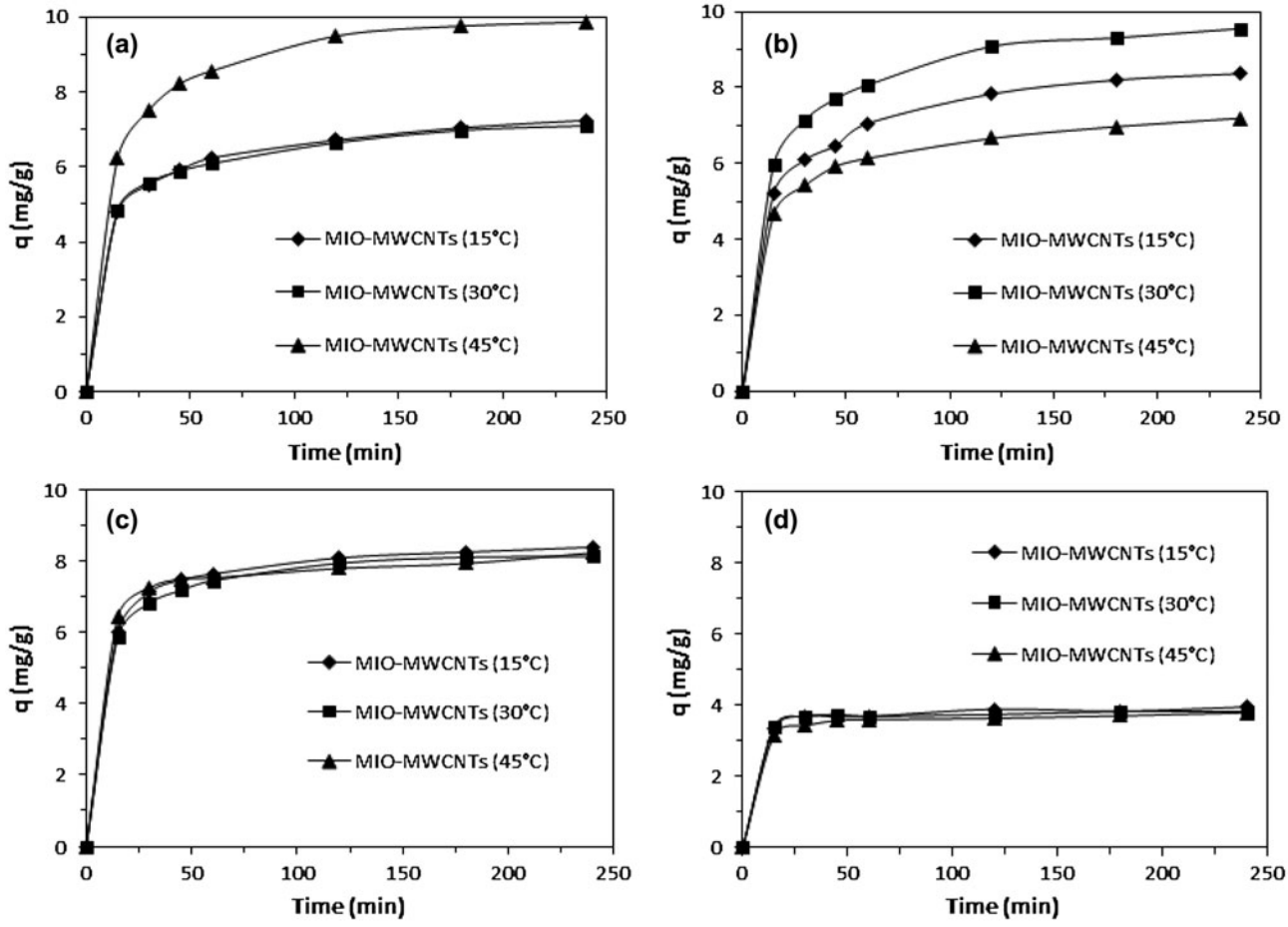

Fig. 6. Arsenic and selenium removal by MIO–MWCNTs at different temperatures: (a) As(III), (b) As(V), (c) Se(IV), and (d) Se(VI).

$$q_t = q_e\left(1 - e^{-k_1 t}\right) \tag{3}$$

$$q_t = \frac{k_2 q_e^2 t}{1 + k_2 q_e t} \tag{4}$$

$$q_t = \frac{1}{\beta}\ln(\alpha\beta) + \frac{1}{\beta}\ln t \tag{5}$$

where q_e is the amount of contaminant adsorbed at equilibrium, q_t is the amount of contaminant adsorbed at time t, k_1 is the pseudo-first-order rate constant, k_2 is the pseudo-second-order rate constant, α is the initial adsorption rate constant, and β is the Elovich adsorption constant.

The kinetic model analyses are presented in Fig. 7. The kinetic model parameters are provided in Table 1. The coefficient of determination (R^2) and the chi-square (χ^2) indicate that the Elovich model was most suitable at describing the arsenic data (Fig. 7(a)). This finding indicates that chemisorption is involved in the adsorption of arsenic to the MIO–MWCNTs. Mishra and Ramaprabhu [38] suggested that the loading of iron oxide on MWCNTs induces chemical reactions. In the case of the selenium data (Fig. 7(b)), the values of R^2 and χ^2 indicate that the pseudo-second-order model was most suitable for describing the kinetic data, which indicates that chemisorption is involved in the adsorption of selenium to the MIO–MWCNTs.

The experimental data in Fig. 6 were also analyzed using the following relationships:

$$\Delta G^\circ = \Delta H^\circ - T\Delta S^\circ \tag{6}$$

$$\Delta G^\circ = -RT\ln K_e;\ K_e = \frac{aq_e}{C_e} \tag{7}$$

$$\ln(K_e) = \frac{\Delta S^\circ}{R} - \frac{\Delta H^\circ}{RT} \tag{8}$$

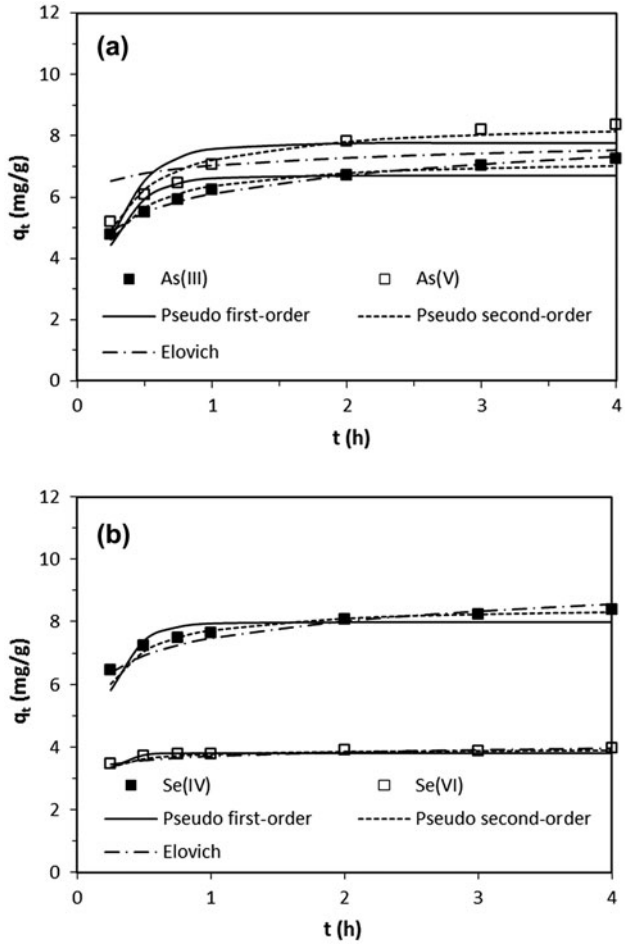

Fig. 7. Kinetic model analyses for reaction time data at 15°C with pseudo-first-order, pseudo-second-order, and Elovich models: (a) arsenic and (b) selenium. Model parameters are provided in Table 1.

where ΔG° is the change in Gibb's free energy, ΔS° is the change in entropy, ΔH° is the change in enthalpy, R is the gas constant, K_e is the equilibrium constant (dimensionless), and a is the adsorbent dose (g/L). ΔS° and ΔH° were calculated by plotting $\ln(K_e)$ vs. $1/T$ using Eq. (8), whereas ΔG° was determined from Eq. (6). The thermodynamic analyses for arsenic and selenium sorption to the MIO–MWCNTs are presented in Fig. 8. The thermodynamic parameters are provided in Table 2.

The thermodynamic behavior of As(III) and As(V) was different (Fig. 8(a)). In the case of As(III), the positive values of ΔH° (56.930 kJ/mol) and ΔS° (204.511 J/K mol) were obtained, indicating that the endothermic and randomness increased at the interface between solid and solution during the sorption process. The positive ΔS° value suggests some structural changes in the arsenic species and adsorbents [39]. For As(V), the negative values of ΔH° (−78.501 kJ/mol) and ΔS° (−238.210 J/K mol) for As(V) demonstrate that the exothermic and randomness decreased during the sorption process. The negative ΔS° value confirms a stable complex forming between As(V) and adsorbents [33]. The negative values of ΔG° (−2.000 to −9.861 kJ/mol) indicate that the sorption process of arsenic on the MIO-MWCNTs was spontaneous.

In the case of Se(IV) and Se(VI) (Fig. 8(b)), the negative values of ΔH° (Se(IV) = −6.921 kJ/mol; Se(VI) = −1.599 kJ/mol) demonstrate the exothermic nature of the sorption process. The negative values of ΔS° (Se(IV) = −9.474 J/K/mol; Se(VI) = −9.178 J/K/mol) indicate that randomness decreased at the interface between solid and solution during the sorption process. The negative values of ΔG° (−3.907 to −4.191 kJ/mol) for Se(IV) show that Se(IV) adsorption to the MIO–MWCNTs was spontaneous. These results are in agreement with reports from other researchers who examined the exothermic and spontaneous adsorption of Se(IV) to titanium dioxide nanoparticles [40] and biosorbent (dead green algae) [41]. In the case of Se(VI), positive values of ΔG° (1.046 to 1.321 kJ/mol) were obtained from the analysis. Similar findings were reported by Jordan et al. [42], who found negative values of ΔH° and ΔS° and a positive value of ΔG° for Se(VI) sorption to anatase. According to Eq. (7), the value of ΔG° becomes positive when the amount of adsorbate in aqueous phase (C_e) is larger than that on solid phase (aq_e) at equilibrium [43]. Özer et al. [44] stated that the sorption reaction would always occur until equilibrium is reached regardless of the sign of ΔG°.

3.4. Effect of solution pH, initial contaminant concentration, and interfering anions

The effect of solution pH on the removal of As(III) and As(V) by the MIO–MWCNTs is presented in Fig. 9(a). Arsenic sorption by the MIO–MWCNTs was clearly affected by the solution pH. The adsorption capacity of As(V) was higher than As(III) at an acidic condition, whereas the adsorption capacity of As(III) was higher at a basic condition. In the adsorption of As(III) to the MIO–MWCNTs, the adsorption capacity increased gradually from 4.25 to 6.95 mg/g between pH 1.6 and 6.8. For As(V), the adsorption capacity at pH 1.7 and 2.8 were above 9.0 mg/g and later dropped gradually to 3.69 mg/g as the pH increased to 7.9. Similar results were revealed in the literature. Brechbühl et al. [45] showed that the sorption of As(III) increased with the increase in pH, while the sorption of As(V) decreased with the pH increase in hematite at a pH range of 3–7. Zhou et al. [46] found the

Table 1
Kinetic model parameters obtained from model fitting to experimental data

		Pseudo-first-order model				Pseudo-second-order model				Elovich model			
	Temperature (℃)	q_e (mg/g)	k_1 (1/h)	R^2	χ^2	q_e (mg/g)	k_2 (g/mg/h)	R^2	χ^2	α (mg/g/h)	β (g/mg)	R^2	χ^2
As(III)	15	6.702	4.347	0.758	0.185	7.275	0.953	0.964	0.027	9.04E+02	1.135	0.992	0.006
	30	6.592	4.676	0.729	0.175	7.127	1.075	0.956	0.028	1.42E+03	1.230	0.993	0.005
	45	9.350	3.817	0.856	0.191	10.212	0.576	0.991	0.012	3.74E+05	1.567	0.967	0.383
As(V)	15	7.764	3.692	0.772	0.288	8.519	0.646	0.958	0.054	9.42E+07	2.756	0.991	0.581
	30	8.927	3.781	0.816	0.243	9.770	0.587	0.978	0.028	3.99E+11	3.433	0.983	0.774
	45	6.659	4.159	0.790	0.173	7.245	0.903	0.973	0.022	1.09E+07	2.819	0.988	0.302
Se(IV)	15	7.987	5.209	0.860	0.074	8.525	1.122	0.995	0.002	1.03E+04	1.269	0.927	0.042
	30	7.776	5.156	0.821	0.099	8.315	1.117	0.993	0.004	7.43E+03	1.260	0.946	0.030
	45	7.771	6.761	0.786	0.055	8.149	1.838	0.962	0.009	3.74E+05	1.801	0.922	0.022
Se(VI)	15	3.799	8.397	0.725	0.017	3.928	5.947	0.906	0.006	9.42E+07	5.417	0.869	0.009
	30	3.757	9.483	0.873	0.004	3.843	8.902	0.918	0.003	3.99E+11	7.801	0.763	0.008
	45	3.640	7.725	0.802	0.015	3.779	5.283	0.971	0.002	1.09E+07	5.050	0.891	0.008

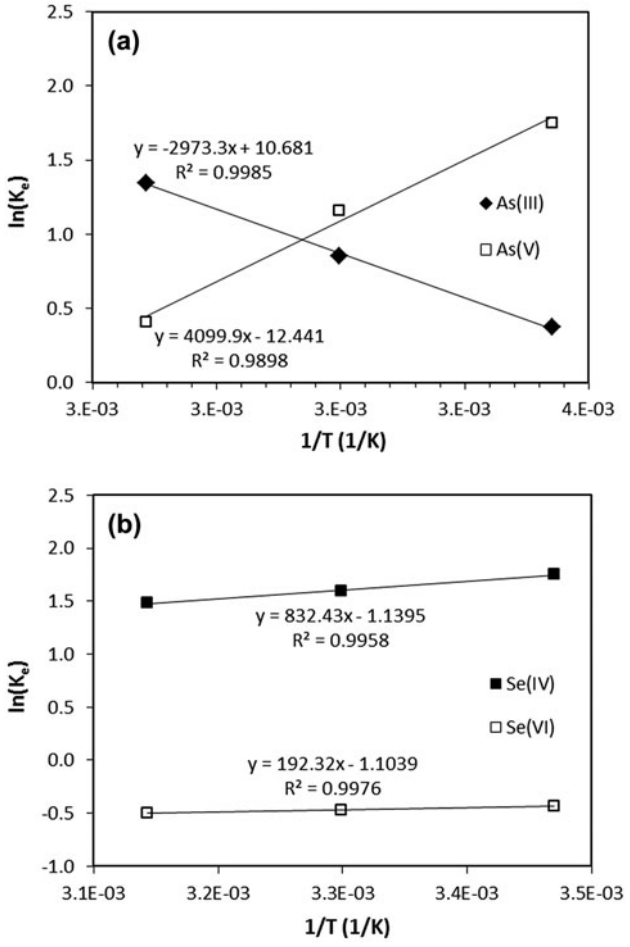

Fig. 8. Thermodynamic model analyses: (a) arsenic and (b) selenium. Model parameters are provided in Table 2.

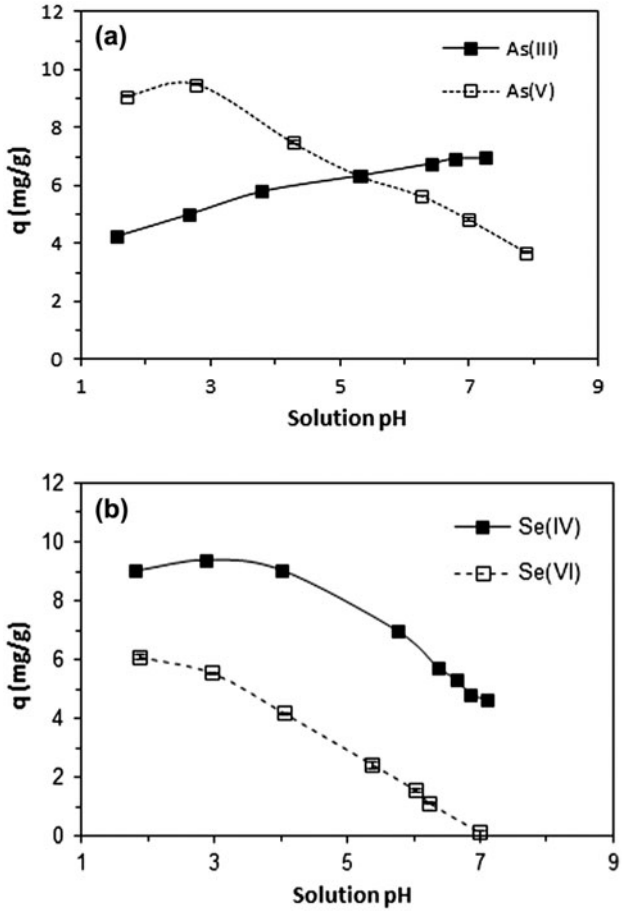

Fig. 9. Arsenic and selenium removal by MIO–MWCNTs at different solution pHs: (a) arsenic and (b) selenium.

Table 2
Thermodynamic parameters obtained from model fitting to experimental data

	Temperature (℃)	ΔH° (kJ/mol)	ΔS° (J/K/mol)	ΔG° (kJ/mol)
As(III)	15	56.930	204.511	−2.000
	30			−5.067
	45			−8.135
As(V)	15	−78.501	−238.210	−9.861
	30			−6.288
	45			−2.715
Se(IV)	15	−6.921	−9.474	−4.191
	30			−4.049
	45			−3.907
Se(VI)	15	−1.599	−9.178	1.046
	30			1.183
	45			1.321

optimal adsorption of As(III) by magnetic cellulose nanocomposites in the pH range of 6–9. Vitela-Rodriguez and Rangel-Mendez [47] reported that the As(V) removal by activated carbon modified with iron hydro (oxide) nanoparticles decreased by 32% as the solution pH increased from 6 to 8.

The chemical speciation of As(III) and As(V) according to the solution pH are calculated by a computer program for geochemical modeling (arsenic concentration = 10 mg/L, temperature = 30˚C, calculation using the Visual MINTEQ 3.0 code):

$$H_3AsO_{3(aq)} \leftrightarrow H_2AsO_3^- + H^+ \quad pK_{a1} = 9.1 \tag{9}$$

$$H_3AsO_{4(aq)} \leftrightarrow H_2AsO_4^- + H^+ \quad pK_{a1} = 2.3 \tag{10}$$

$$H_2AsO_4^- \leftrightarrow HAsO_4^{2-} + H^+ \quad pK_{a2} = 6.9 \tag{11}$$

In our experimental condition (pH 3), $H_2AsO_4^-$ (monovalent anion) is the predominant form of As(V). The anionic species of As(V) is strongly influenced by the surface charge of the adsorbent. Under acidic condition, the surface of the adsorbents becomes positively charged by protonation, subsequently enhancing the adsorption of negatively charged As(V). As the solution pH increases, the surface of the adsorbents is deprotonated and becomes unfavorable for the adsorption of As(V) [9,48]. For As(III), H_2AsO_3 (neutral species) is the predominant form in our experimental condition (pH 7). The neutral species of As(III) is not affected by the surface charge of the adsorbents. The magnetic iron oxide on CNTs is partially dissolved at a low pH condition, which can cause a reduction in As(III) adsorption. The higher removal capacity of As(III) at a basic condition may be the result of oxidation of arsenite to arsenate [46,48].

The influence of solution pH on the removal of Se (IV) and Se(VI) by the MIO–MWCNTs are shown in Fig. 9(b). Selenium sorption by the MIO–MWCNTs was influenced by the solution pH. In the case of Se (IV), the adsorption capacity was 9.40 mg/g at pH 1.8 and dropped gradually to 4.65 mg/g as the pH was increased to 7.1. The adsorption capacity of Se(VI) also decreased gradually from 6.09 to 0.11 mg/g with a rise in pH from 1.9 to 7.0. At the same pH, the adsorption capacity of Se(IV) was larger than that of Se(VI). Similar findings were reported by Martínez et al. [30], who showed that the percent removal of Se (IV) by magnetite decreased from 55 to 3% upon increasing the pH from 2 to 12, whereas the percent removal of Se(VI) decreased from 12 to 1% at the same pH range.

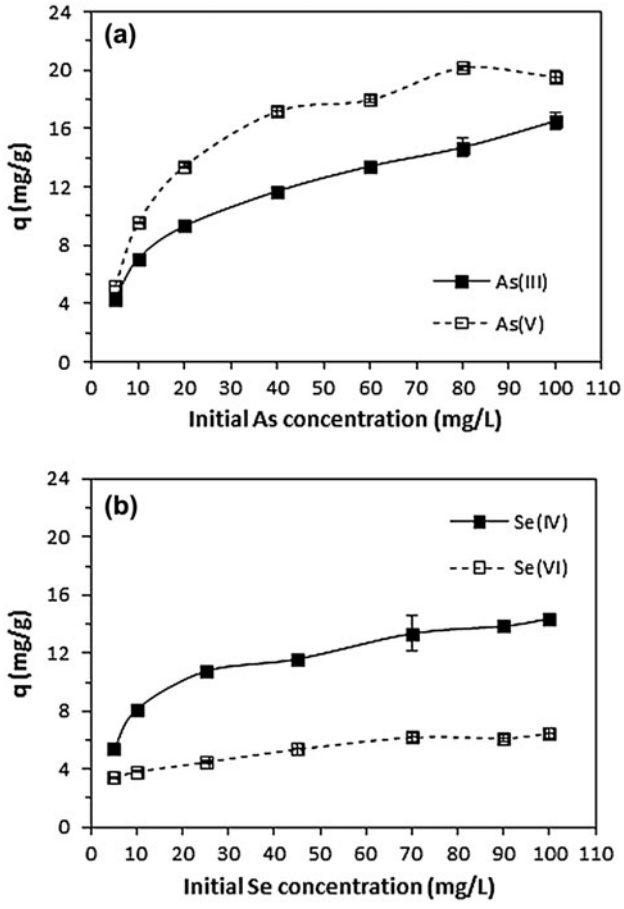

Fig. 10. Arsenic and selenium removal by MIO–MWCNTs at different initial contaminant concentrations: (a) arsenic and (b) selenium.

The pH dependency of adsorption of Se(IV) and Se (VI) to the MIO–MWCNTs is primarily related to the ionization of selenium. The speciation of Se(IV) and Se (VI) is influenced by the solution pH (selenium concentration = 10 mg/L, temperature = 30˚C, calculation using the Visual MINTEQ 3.0 code):

$$H_2SeO_{3(aq)} \leftrightarrow HSeO_3^- + H^+ \quad pK_{a1} = 2.63 \tag{12}$$

$$HSeO_3^- \leftrightarrow SeO_3^{2-} + H^+ \quad pK_{a2} = 8.36 \tag{13}$$

$$HSeO_4^- \leftrightarrow SeO_4^{2-} + H^+ \quad pK_{a1} = 1.61 \tag{14}$$

In our experimental condition (pH 4), $HSeO_3^-$ (monovalent anion) is the predominant form of Se(IV), whereas SeO_4^{2-} (divalent anion) is the predominant form of Se(VI). Like As(V), the anionic species of Se(IV) and Se(VI) are strongly influenced by the surface charge of the adsorbent.

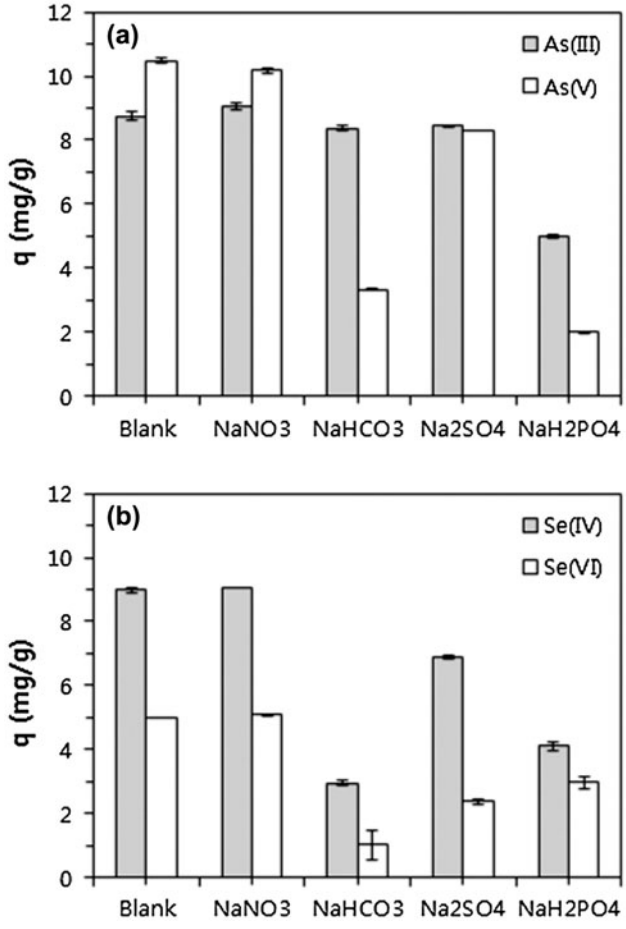

Fig. 11. Arsenic and selenium removal by MIO–MWCNTs at various interfering anions: (a) arsenic and (b) selenium.

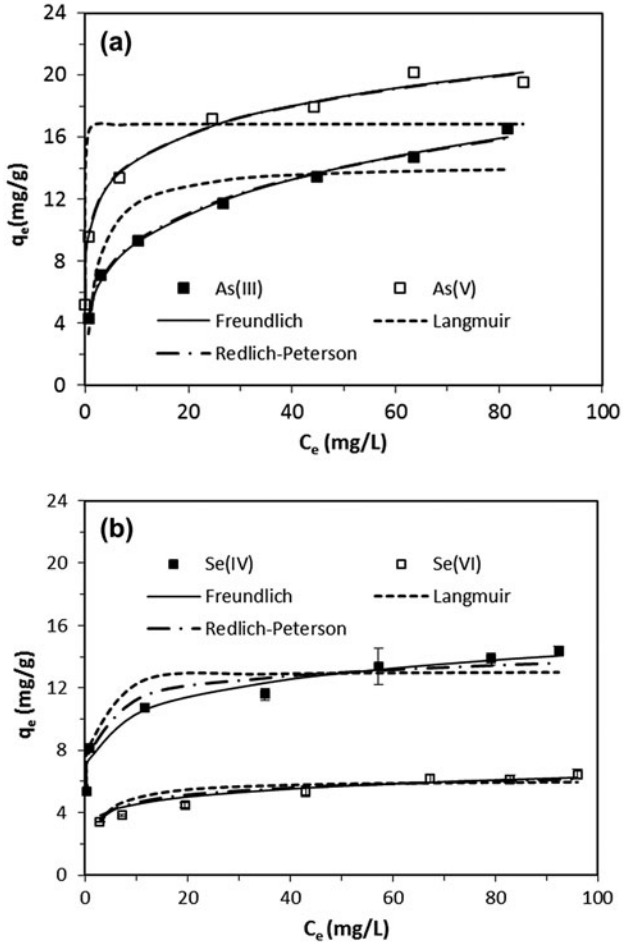

Fig. 12. Equilibrium isotherm model analyses with the Freundlich, Langmuir, and Redlich–Peterson models: (a) arsenic and (b) selenium. Model parameters are provided in Table 3.

The removal of As(III) and As(V) by the MIO–MWCNTs is presented in Fig. 10(a) as a function of initial arsenic concentration. The adsorption capacity increased gradually with increasing initial arsenic concentrations. In the case of As(III), the adsorption capacity at the concentration of 5 mg/L was 4.32 mg/g. The adsorption capacity increased to 11.71 mg/g at the concentration of 40 mg/L and further increased to 16.52 mg/g at the highest concentration of 100 mg/L. Meanwhile, the adsorption capacity of As(V) increased from 5.19 to 19.54 mg/g with increasing As(V) concentrations from 5 to 100 mg/L. These results also show that the adsorption capacity of As(V) was greater than that of As(III) throughout the initial arsenic concentration.

The removal of Se(IV) and Se(VI) by the MIO–MWCNTs is shown in Fig. 10(b) as a function of initial selenium concentration. In the case of Se(IV), the adsorption capacity at the concentration of 5 mg/L was 5.37 mg/g, which increased to 11.59 mg/g with the concentration of 45 mg/L. The adsorption capacity further increased to 14.37 mg/g with the concentration of 100 mg/L. For Se(VI), the adsorption capacity increased from 3.40 to 6.47 mg/g with a rise in the concentration from 5 to 100 mg/L. Our results show that the adsorption capacity of Se(IV) was greater than that of Se(VI) throughout the initial selenium concentration.

The effect of interfering anions on the removal of arsenic and selenium by the MIO–MWCNTs are presented in Fig. 11. In the case of As(III), nitrate, bicarbonate, and sulfate did not significantly influence on the As(III) removal while phosphate interfered As(III) removal. In the case of As(V), both carbonate and phosphate greatly reduced the As(V) removal. Rao et al. [49] reported that arsenic removal by Fe–Ti

Table 3
Equilibrium isotherm model parameters obtained from model fitting to experimental data

	Freundlich model				Langmuir model				Redlich–Peterson model				
	K_F (L/g)	$1/n$	R^2	χ^2	Q_m (mg/g)	K_L (L/mg)	R^2	χ^2	K_R (L/g)	a_R (L/mg)	K_R/a_R (mg/g)	g	R^2	χ^2
As(III)	5.019	0.264	0.995	0.055	14.263	0.462	0.836	1.736	92.774	17.640	5.259	0.748	0.994	0.050
As(V)	10.285	0.152	0.992	0.083	16.847	41.212	0.602	4.620	35,433.87	3,431.78	10.325	0.849	0.992	0.086
Se(IV)	7.573	0.137	0.904	0.671	13.081	1.962	0.870	0.641	43.248	4.381	9.872	0.928	0.923	0.417
Se(VI)	3.298	0.140	0.829	0.274	6.130	0.444	0.754	0.323	6.608	1.624	4.069	0.906	0.831	0.263

bimetal oxides decreased significantly due to the presence of phosphate. In the case of Se(IV), the influence of interfering anions was in the order of bicarbonate > phosphate > sulfate. In the case of Se(VI), the effect was in the order of bicarbonate > sulfate > phosphate. Note that nitrate did not interfere the selenium removal.

3.5. Equilibrium isotherm model analysis

The sorption data in Fig. 10 were analyzed with the Freundlich (Eq. (15)), Langmuir (Eq. (16)), and Redlich–Peterson (Eq. (17)) isotherm models:

$$q_e = K_F C_e^{\frac{1}{n}} \tag{15}$$

$$q_e = \frac{Q_m K_L C_e}{1 + K_L C_e} \tag{16}$$

$$q_e = \frac{K_R C_e}{1 + a_R C_e^g} \tag{17}$$

where C_e is the equilibrium concentration of contaminant in the aqueous solution, K_F is the Freundlich constant related to the adsorption capacity, $1/n$ is the Freundlich constant related to the adsorption intensity, Q_m is the maximum adsorption capacity, K_L is the Langmuir constant related to the affinity of the binding sites, K_R is the Redlich–Peterson constant related to the adsorption capacity, a_R is the Redlich–Peterson constant related to the affinity of the binding sites, and g is the Redlich–Peterson constant related to the adsorption intensity.

The equilibrium model analyses are illustrated in Fig. 12. The equilibrium model parameters are represented in Table 3. The values of R^2 and χ^2 indicate that the Freundlich isotherm was most suitable at describing the arsenic data. The maximum adsorption capacities (Q_m) of As(III) and As(V) were determined to be 14.26 and 16.85 mg/g, respectively, from the Langmuir model, which were higher than the value in the literature. Ma et al. [3] reported that magnetic iron oxide/CNT composites had maximum sorption capacities of 9.74 mg/g for As(V) and 8.13 mg/g for As(III) from the Langmuir isotherm. Ntim and Mitra [9] determined As(III) and As(V) sorption capacities for Fe–MWCNT of 1.72 and 0.19 mg/g, respectively, from the Langmuir isotherm.

In the case of selenium data, the values of R^2 and χ^2 indicate that the Redlich–Peterson isotherm was most suitable for describing the equilibrium data.

The Redlich–Peterson isotherm is a hybrid model combining the Freundlich and Langmuir equations, which can be applied to either homogeneous or heterogeneous systems to explain adsorption over a wide range of concentrations [50]. The values of Q_m for Se (IV) and Se(VI) from the Langmuir model were 13.08 and 6.13 mg/g, respectively, which were in the range of reported values from the literature. Wang et al. [17] reported that Fe–Ni/MWCNT had a Se(IV) sorption capacity of 17.45 mg/g from the Langmuir isotherm. Chan et al. [51] determined Se(IV) and Se(VI) sorption capacities for binary oxides ($Fe(III)/SiO_2$) of 20.4 and 2.4 mg/g, respectively, from the Langmuir isotherm. Zhang et al. [40] reported that the Se(IV) sorption capacities of nano-TiO_2 were 7.30–8.46 mg/g from the Langmuir isotherm. Gonzalez et al. [4] reported that microwave-assisted magnetite nanomaterial had Se(IV) and Se(VI) sorption capacities of 2.38 and 2.37 mg/g, respectively, from the Langmuir isotherm.

4. Conclusions

The removal of arsenic and selenium by the MIO–MWCNTs was examined in this study. Results demonstrate that the MIO–MWCNTs were more effective in the removal of arsenic and selenium than oxidized MWCNTs. Kinetic model analyses demonstrate that the Elovich model was found to be the most suitable for describing the As(III) and As (V) data, whereas the pseudo-second-order model provided the best fit for the Se(IV) and Se(VI) data. Thermodynamic analyses indicate that As(III) adsorption was endothermic, while As(V) adsorption was exothermic. Meanwhile, the adsorption of Se(IV) and Se(VI) was exothermic. Arsenic and selenium adsorption to the MIO–MWCNTs was clearly affected by the solution pH of 2–8. As pH increased, the adsorption capacity of As(III) increased, whereas the adsorption capacity of As(V) decreased. The adsorption capacities of Se(IV) and Se(VI) decreased with a rise in pH. Interfering anions such as phosphate and carbonate significantly reduced the removal of arsenic and selenium. Equilibrium model analyses indicate that the Freundlich model was the most appropriate for the As(III) and As(V) data, whereas the Redlich–Peterson model gave the best fit for the Se(IV) and Se(VI) data. The maximum adsorption capacity from the Langmuir model (mg/g) was in the order of As(V) (16.85) > As(III) (14.26) > Se(IV) (13.08) > Se(VI) (6.13). This study demonstrates that the MIO–MWCNTs can be used as adsorbents for removing arsenic and selenium from water in combination with magnetic separation.

Acknowledgment

This work was supported by the National Research Foundation of Korea, funded by the Ministry of Education, Republic of Korea (grant number 2015–025688).

References

[1] B. An, H. Kim, C. Park, S.H. Lee, J.W. Choi, Preparation and characterization of an organic/inorganic hybrid sorbent (PLE) to enhance selectivity for As(V), J. Hazard. Mater. 289 (2015) 54–62.
[2] C. Wang, H. Luo, Z. Zhang, Y. Wu, J. Zhang, S. Chen, Removal of As(III) and As(V) from aqueous solutions using nanoscale zero valent iron-reduced graphite oxide modified composites, J. Hazard. Mater. 268 (2014) 124–131.
[3] J. Ma, Z. Zhu, B. Chen, M. Yang, H. Zhou, C. Li, F. Yu, J. Chen, One-pot, large-scale synthesis of magnetic activated carbon nanotubes and their applications for arsenic removal, J. Mater. Chem. A 1 (2013) 4662–4666.
[4] C.M. Gonzalez, J. Hernandez, J.R. Peralta-Videa, C.E. Botez, J.G. Parsons, J.L. Gardea-Torresdey, Sorption kinetic study of selenite and selenate onto a high and low pressure aged iron oxide nanomaterial, J. Hazard. Mater. 211–212 (2012) 138–145.
[5] D.S. Han, B. Batchelor, A. Abdel-Wahab, Sorption of selenium(IV) and selenium(VI) to mackinawite (FeS): Effect of contact time, extent of removal, sorption envelopes, J. Hazard. Mater. 186 (2011) 451–457.
[6] M. Rovira, J. Giménez, M. Martínez, X. Martínez-Lladó, J. de Pablo, V. Martí, L. Duro, Sorption of selenium(IV) and selenium(VI) onto natural iron oxides: Goethite and hematite, J. Hazard. Mater. 150 (2008) 279–284.
[7] E.I. El-Shafey, Removal of Se(IV) from aqueous solution using sulphuric acid-treated peanut shell, J. Environ. Manage. 84 (2007) 620–627.
[8] S.C.B. Myneni, T.K. Tokunaga, G.E. Brown Jr., Abiotic selenium redox transformations in the presence of Fe (II, III) oxides, Science 278 (1997) 1106–1109.
[9] S.A. Ntim, S. Mitra, Removal of trace arsenic to meet drinking water standards using iron oxide coated multiwall carbon nanotubes, J. Chem. Eng. Data 56 (2011) 2077–2083.
[10] Z. Veličković, G.D. Vuković, A.D. Marinković, M.S. Moldovan, A.A. Perić-Grujić, P.S. Uskoković, M.D. Ristić, Adsorption of arsenate on iron(III) oxide coated ethylenediamine functionalized multiwall carbon nanotubes, Chem. Eng. J. 181–182 (2012) 174–181.
[11] X. Luo, C. Wang, S. Luo, R. Dong, X. Tu, G. Zeng, Adsorption of As(III) and As(V) from water using magnetite Fe_3O_4-reduced graphite oxide–MnO_2 nanocomposites, Chem. Eng. J. 187 (2012) 45–52.
[12] R. Chen, C. Zhi, H. Yang, Y. Bando, Z. Zhang, N. Sugiur, D. Golberg, Arsenic(V) adsorption on Fe_3O_4 nanoparticle-coated boron nitride nanotubes, J. Colloid Interface Sci. 359 (2011) 261–268.
[13] X. Ren, C. Chen, M. Nagatsu, X. Wang, Carbon nanotubes as adsorbents in environmental pollution management: A review, Chem. Eng. J. 170 (2011) 395–410.

[14] V.K. Gupta, T.A. Saleh, Sorption of pollutants by porous carbon, carbon nanotubes and fullerene—An overview, Environ. Sci. Pollut. Res. 20 (2013) 2828–2843.
[15] S. Zeng, Y. Cao, W. Sang, T. Li, N. Gan, L. Zheng, Enrichment of polychlorinated biphenyls from aqueous solutions using Fe_3O_4 grafted multiwalled carbon nanotubes with poly dimethyl diallyl ammonium chloride, Int. J. Mol. Sci. 13 (2012) 6382–6398.
[16] B.S. Tawabini, S.F. Al-Khaldi, M.M. Khaled, M.A. Atieh, Removal of arsenic from water by iron oxide nanoparticles impregnated on carbon nanotubes, J. Environ. Sci. Health, Part A 46 (2011) 215–223.
[17] Y.S. Wang, S.H. Hsieh, C.H. Lee, J.J. Horng, Adsorption of complex pollutants from aqueous solutions by nanocomposite materials, Clean—Soil, Air, Water 41 (2013) 574–580.
[18] L. Ji, L. Zhou, X. Bai, Y. Shao, G. Zhao, Y. Qu, C. Wang, Y. Li, Facile synthesis of multiwall carbon nanotubes/iron oxides for removal of tetrabromobisphenol A and Pb(II), J. Mater. Chem. 22 (2012) 15853–15862.
[19] V.K. Gupta, S. Agarwal, T.A. Saleh, Chromium removal by combining the magnetic properties of iron oxide with adsorption properties of carbon nanotubes, Water Res. 45 (2011) 2207–2212.
[20] R. Chen, L. Chai, Q. Li, Y. Shi, Y. Wang, A. Mohammad, Preparation and characterization of magnetic Fe_3O_4/CNT nanoparticles by RPO method to enhance the efficient removal of Cr(VI), Environ. Sci. Pollut. Res. 20 (2013) 7175–7185.
[21] B. Chen, Z. Zhu, J. Ma, M. Yang, J. Hong, X. Hu, Y. Qiu, J. Chen, One-pot, solid-phase synthesis of magnetic multiwalled carbon nanotube/iron oxide composites and their application in arsenic removal, J. Colloid Interface Sci. 434 (2014) 9–17.
[22] M.A. Bavio, A.G. Lista, Synthesis and characterization of hybrid-magnetic nanoparticles and their application for removal of arsenic from groundwater, Sci. World J. 2013 (2013) 1–7.
[23] L. Ai, C. Zhang, F. Liao, Y. Wang, M. Li, L. Meng, J. Jiang, Removal of methylene blue from aqueous solution with magnetite loaded multi-wall carbon nanotube: Kinetic, isotherm and mechanism analysis, J. Hazard. Mater. 198 (2011) 282–290.
[24] S.Y. Yoon, C.G. Lee, J.A. Park, J.H. Kim, S.B. Kim, S.H. Lee, J.W. Choi, Kinetic, equilibrium and thermodynamic studies for phosphate adsorption to magnetic iron oxide nanoparticles, Chem. Eng. J. 236 (2014) 341–347.
[25] C.G. Lee, S.B. Kim, Cr(VI) adsorption to magnetic iron oxide nanoparticle-multi-walled carbon nanotube adsorbents, Water Environ. Res. 88 (in press).
[26] Z. Sun, Z. Liu, Y. Wang, B. Han, J. Du, J. Zhang, Fabrication and characterization of magnetic carbon nanotube composites, J. Mater. Chem. 15 (2005) 4497–4501.
[27] I.T. Kim, G.A. Nunnery, K. Jacob, J. Schwartz, X. Liu, R. Tannenbaum, Synthesis, characterization, and alignment of magnetic carbon nanotubes tethered with maghemite nanoparticles, J. Phys. Chem. C 114 (2010) 6944–6951.
[28] W. Yan, M.A.V. Ramos, B.E. Koel, W. Zhang, Multitiered distributions of arsenic in iron nanoparticles: Observation of dual redox functionality enabled by a core–shell structure, Chem. Commun. 46 (2010) 6995–6997.
[29] A. Naveau, F. Monteil-Rivera, E. Guillon, J. Dumonceau, Interactions of aqueous selenium (−II) and (IV) with metallic sulfide surfaces, Environ. Sci. Technol. 41 (2007) 5376–5382.
[30] M. Martínez, J. Giménez, J. de Pablo, M. Rovira, L. Duro, Sorption of selenium(IV) and selenium(VI) onto magnetite, Appl. Surf. Sci. 252 (2006) 3767–3773.
[31] L. Zeng, Arsenic adsorption from aqueous solutions on an Fe(III)–Si binary oxide adsorbent, Water Qual. Res. J. Canada 39 (2004) 267–275.
[32] H.S. Altundoğan, S. Altundoğan, F. Tümen, M. Bildik, Arsenic adsorption from aqueous solutions by activated red mud, Waste Manage. (Oxford) 22 (2002) 357–363.
[33] A.O.A. Tuna, E. Özdemir, E.B. Şimşek, U. Beker, Removal of As(V) from aqueous solution by activated carbon-based hybrid adsorbents: Impact of experimental conditions, Chem. Eng. J. 223 (2013) 116–128.
[34] M.A. Sabur, S. Goldberg, A. Gale, N. Kabengi, H.A. Al-Abadleh, Temperature-dependent infrared and calorimetric studies on arsenicals adsorption from solution to hematite nanoparticles, Langmuir 31 (2015) 2749–2760.
[35] R.R. Sheha, E.A. El-Shazly, Kinetics and equilibrium modeling of Se(IV) removal from aqueous solutions using metal oxides, Chem. Eng. J. 160 (2010) 63–71.
[36] J.H. Kwon, L.D. Wilson, R. Sammynaiken, Sorptive uptake of selenium with magnetite and its supported materials onto activated carbon, J. Colloid Interface Sci. 457 (2015) 388–397.
[37] M. Kersten, N. Vlasova, The influence of temperature on selenate adsorption by goethite, Radiochim. Acta 101 (2013) 413–420.
[38] A.K. Mishra, S. Ramaprabhu, Magnetite decorated multiwalled carbon nanotube based supercapacitor for arsenic removal and desalination of seawater, J. Phys. Chem. C 114 (2010) 2583–2590.
[39] F. Partey, D. Norman, S. Ndur, R. Nartey, Arsenic sorption onto laterite iron concretions: Temperature effect, J. Colloid Interface Sci. 321 (2008) 493–500.
[40] L. Zhang, N. Liu, L. Yang, Q. Lin, Sorption behavior of nano-TiO_2 for the removal of selenium ions from aqueous solution, J. Hazard. Mater. 170 (2009) 1197–1203.
[41] M. Tuzen, A. Sarı, Biosorption of selenium from aqueous solution by green algae (*Cladophora hutchinsiae*) biomass: Equilibrium, thermodynamic and kinetic studies, Chem. Eng. J. 158 (2010) 200–206.
[42] N. Jordan, K. Müller, C. Franzen, V. Brendler, Temperature impact on the sorption of selenium(VI) onto anatase, J. Colloid Interface Sci. 390 (2013) 170–175.
[43] D. Karadag, E. Akgul, S. Tok, F. Erturk, M.A. Kaya, M. Turan, Basic and reactive dye removal using natural and modified zeolites, J. Chem. Eng. Data 52 (2007) 2436–2441.
[44] A. Özer, G. Akkaya, M. Turabik, The biosorption of acid red 337 and acid blue 324 on *Enteromorpha prolifera*: The application of nonlinear regression analysis to dye biosorption, Chem. Eng. J. 112 (2005) 181–190.
[45] Y. Brechbühl, I. Christl, E.J. Elzinga, R. Kretzschmar, Competitive sorption of carbonate and arsenic to hematite: Combined ATR-FTIR and batch experiments, J. Colloid Interface Sci. 377 (2012) 313–321.

[46] S. Zhou, D. Wang, H. Sun, J. Chen, S. Wu, P. Na, Synthesis, characterization, and adsorptive properties of magnetic cellulose nanocomposites for arsenic removal, Water, Air, Soil Pollut. 225 (2014) 1945.
[47] A.V. Vitela-Rodriguez, J.R. Rangel-Mendez, Arsenic removal by modified activated carbons with iron hydro(oxide) nanoparticles, J. Environ. Manage. 114 (2013) 225–231.
[48] D. Ociński, I. Jacukowicz-Sobala, J. Raczyk, E. Kociołek-Balawejder, Evaluation of hybrid polymer containing iron oxides as As(III) and As(V) sorbent for drinking water purification, React. Funct. Polym. 83 (2014) 24–32.
[49] P. Rao, Z. Sun, W. Zhang, W. Yao, L. Wang, G. Ding, Preparation and application of amorphous Fe–Ti bimetal oxides for arsenic removal, RSC Adv. 5 (2015) 89545–89551.
[50] K.Y. Foo, B.H. Hameed, Insights into the modeling of adsorption isotherm systems, Chem. Eng. J. 156 (2010) 2–10.
[51] Y.T. Chan, W.H. Kuan, T.Y. Chen, M.K. Wang, Adsorption mechanism of selenate and selenite on the binary oxide systems, Water Res. 43 (2009) 4412–4420.